RSC Advances

ROYAL SOCIETY OF CHEMISTRY

www.rsc.org/advances

Cite this: DOI: 10.1039/c0xx00000x

www.rsc.org/xxxxxx

ARTICLE TYPE

Role of multiwalled carbon nanotubes (MWCNTs) on rheological, thermal and electrical properties of PC/ABS blend

Amir Rostami,*[a, b] Mohsen Masoomi,[a] Mohammad Javad Fayazi[a] and Mehdi Vahdati[b]

Received (in XXX, XXX) Xth XXXXXXXXX 20XX, Accepted Xth XXXXXXXXX 20XX

DOI: 10.1039/b000000x

The main objective of this work was to probe the effect of multiwalled carbon nanotubes (MWCNTs) on the rheological, electrical and thermal properties of polycarbonate (PC)/acrylonitrile butadiene styrene (ABS) 75/25 blend prepared by simultaneous melt blending. The results of thermodynamics measurements suggested that the MWCNTs were preferentially localized in the interface of the PC and ABS; however, melt linear viscoelastic measurements and TEM results showed a greater affinity of MWCNTs towards the PC matrix. This was also supported by the electrical percolation threshold observed at low MWCNTs content. The microstructure of the samples was analyzed by melt linear viscoelastic experiments and electron microscopy, which revealed that the MWCNTs were dispersed quite homogeneously in the PC matrix. The electrical conductivity and electromagnetic interference shielding efficiency (EMI SE) of the blend nanocomposite samples were enhanced with increasing the loading level of MWCNTs. Finally, thermal analysis was employed as a complementary experiment to provide further evidence for MWCNTs' partitioning.

Introduction

Polymer blending is among the successful methods of producing new polymers/products with desirable/tailored properties. Among the polymer blends, PC/ABS has received special attention for its wide range of industrial applications, due to the combination of the high thermal stability and good impact behavior of PC and easy processability of ABS. Furthermore, PC notch sensitivity is improved by the addition of ABS.[1-7]

The change from microsized fillers to nanofillers has proved to be a promising method to produce composites of dramatically enhanced physical and mechanical properties by using much lower nanofiller loading levels.[8] How far these goals are achieved depends heavily on the state of dispersion and microstructure of the polymer nanocomposites. The interfacial interaction between nanofillers and the polymer matrix is the most important factor involved in determining the state of nanofiller dispersion.[9-12]

Ever since Ajayan et al.[10] used carbon nanotubes as fillers in a polymer nanocomposite for the first time, numerous papers have been published on carbon nanotubes filled nanocomposites, which attempted to achieve a fair combination of enhanced mechanical, electrical, thermal, and other properties.[13-15]

Over the past decade, increasing activities have been directed towards using conductive nanofillers, such as carbon nanotubes and graphite nanosheets, in polymer blends. Electrical properties of polymer blend nanocomposites are a function of nanofiller characteristics (purity, aspect ratio, etc.), blend morphology (matrix/dispersed, co-continuous, etc.) and nanofiller localization. Given a homogenous dispersion, high purity and aspect ratio of nanofiller cause enhanced electrical conductivity at relatively low nanofiller loading levels.[16-34] It has been shown that localization (partitioning) of nanofillers plays a key role in determining the morphology and nanoscopic structure, hence, controlling the physical and mechanical performance of such hybrid systems.

The localization of nanofillers in polymer blends has been suggested to be governed by two types of parameters: a) thermodynamic parameters, including interfacial tension between the nanofillers and the polymer components; b) kinetic parameters, which are controlled by the viscosity of the polymer components, composition, mixing sequence and processing conditions (temperature, shear rate and mixing time).[35-37] In the case of blend nanocomposites with matrix/dispersed morphology, if nanofillers are selectively localized in the matrix, the percolation threshold decreases compared to corresponding single polymer based nanocomposites.[21, 33] On the other hand, if the nanofillers tend to localize in the dispersed phase, the sample is non-conductive unless the dispersed phase is sufficiently fine to allow tunneling effects to occur.[38] In the case of blend nanocomposites with co-continuous morphology, if the nanofillers selectively localize in one blend component (the so-called double percolation concept) or at the interface, the lowest percolation threshold is obtained.[17, 20, 39]

Carbon nanotubes filled PC/ABS blends have been studied by a number of researchers.[40-45] Sun et al.[40], for instance, have shown that localization of MWCNTs changed from the PC to the ABS phase when rubber content of ABS was varied from 5% to 60%. They showed that at low contents of the rubber ABS, the MWCNTs are selectively localized in the PC phase and conductive nanocomposite samples were achieved. Maiti et al.[42] have reported the percolation threshold at 0.195 vol% of MWCNTs loading level in the PC matrix, prepared by melt dilution of the ABS-MWCNTs. Xiong et al.[41] have studied the migration or controlled location of MWCNTs by a combination of morphology evolution, rubber content, and MWCNTs higher affinity to PB than to PC. Their study indicated selective localization of most MWCNTs in the continuous ABS phase; however, with increased mixing time, most MWCNTs returned to the PC. Taheri et al.[43] have reported that MWCNTs were localized in the ABS phase. They have also shown that in

addition to the relative affinity of the MWCNTs towards the blend components, the MWCNTs concentration could also play a role in determining the MWCNTs partitioning. Monemian et al.[44] have observed a selective localization of MWCNT within the PC phase and a low electrical percolation threshold due to double percolation phenomenon. Han et al.[45] have shown that MWCNTs are localized in ABS phase and that the electrical conductivity was higher for nanocomposites with SAN-g-MAH as a compatibilizer. The different thermodynamic and kinetic conditions employed in some of these works are responsible for the apparent contradictions observed. Therefore, more work is required to gain an adequate understanding of the localization of MWCNTs in PC/ABS blend.

Melt rheological properties of polymer nanocomposites are very sensitive to their microstructure, including the state of dispersion of nanofillers in the matrix. Thus, rheology can be used as a suitable tool to study the microstructure of polymer nanocomposites. Moreover, rheological measurements provide valuable information to optimize the melt processing conditions for achieving high performance polymer nanocomposites.[46, 47]

In this work, we investigated MWCNTs localization and its impact on rheological, electrical, and thermal properties of PC/ABS(75/25)/MWCNTs blend nanocomposites.

Experimental

Materials

Polycarbonate (PC) from Bayer Co., Germany and Acrylonitrile Butadiene Styrene (ABS) from Tabriz Petrochemical Co., Iran, were used in this work. The properties of these polymers are listed in Table 1. The carbon nanotubes used in this study were commercially available as multiwall carbon nanotubes (MWCNTs), NC-7000, from Nanocyl Inc., Belgium. The MWCNTs had a carbon purity of 90%, average outer diameter of 9.5 nm, length up to 1.5 μm, and surface area of 250–300 m^2/g. An SEM micrograph of the MWCNTs is shown in Fig. 1.

Sample preparation

PC/ABS blends, with a composition of 75/25 wt.%, were prepared with three different concentrations of MWCNTs (i.e., 0.5, 1 and 1.5 wt.%, based on the blend mass), using simultaneous melt mixing in a laboratory Brabender internal mixer (D-47055, Germany) at 260 °C for a total mixing time of 12 minutes. For the DMTA and electrical measurements, a portion of the mixed material from the internal mixer was ground into small pieces and compression molded into rectangular shaped moldings by using a Ceast compression molding machine (Italy) for 8 minutes at 260 °C under a molding pressure of 35 MPa, followed by slow water-cooling.

Characterization methods

Surface tension measurements were carried out using a contact angle method utilizing a KRUSS K14 Tensiometer (Germany) at 25 °C with extrapolation to the processing temperature using the values of temperature coefficient of surface tension ($d\gamma/dT$).[48]

The oscillatory shear rheological measurements were carried out at 260 °C using an MCR 301 rheometer (Physica Anton Paar, Austria) using parallel plate geometry, with a diameter of 25 mm and a gap of 1 mm. The dynamic strain amplitude sweep experiments were performed for determination of the linear viscoelastic region by monitoring the storage modulus. Melt linear viscoelastic behavior of the samples was studied using frequency sweep experiments with small strain oscillatory shear deformations.

The morphology of the samples was examined by using scanning electron microscopy (SEM), with an AIS-2100 from Seron Co. (South Korea) at 15 kV. Acid etching of the cryogenically fractured surface was carried out in order to etch out the ABS dispersed phase and the resulting samples were coated with gold using a sputter coater under argon gas atmosphere. Furthermore, ultrathin sections (~200 nm) of the samples were prepared by an ultramicrotome and transmission electron microscopy (TEM) images were taken using a Philips EM 208S (Netherlands) with a voltage of 120 kV.

The volume resistivity measurements were performed on rectangular shaped compression molded samples (10×10 cm^2, thickness of 2 mm) using a Ceast Teraohm meter (Italy). The samples' surface was covered with silver paste to ensure good contact with the electrodes. The resistivity was converted to volume resistivity according to ASTM D257. The electromagnetic interference shielding efficiency (EMI SE) of the blend nanocomposites was measured using HP 8410C Network Analyzer (Japan) in the frequency range of 5–12 GHz; the sample thickness was 2 mm.

Dynamic mechanical thermal analyses of the compression molded samples were performed at a frequency of 1.0 Hz and a heating rate of 3 °C/min using a Perkin-Elmer Pyris Diamond DMTA dynamic mechanical analyzer (USA). Thermogravimetric analysis curves were recorded with a Perkin-Elmer Pyris Diamond TG/DTA Thermogravimetric/Differential Thermal Analyzer (USA). The samples were heated from 50 to 600 °C at a heating rate of 10 °C/min under nitrogen atmosphere.

Results and discussion

Thermodynamic description of the MWCNTs localization in the blend samples

The thermodynamic preference of a nanofiller to distribute selectively can be predicted by describing wetting coefficient, ω_a a simple mathematical description of this thermodynamic tendency[49]:

$$\omega_a = \frac{\gamma_{MWCNTs-PC} - \gamma_{MWCNTs-ABS}}{\gamma_{ABS-PC}} \quad (1)$$

where $\gamma_{MWCNTs-PC}$ and $\gamma_{MWCNTs-ABS}$ are the interfacial tensions between the MWCNTs and the PC and ABS, respectively, and γ_{ABS-PC} represents the interfacial tension between the PC and ABS. If $\omega_a>1$, the MWCNTs are located within the PC phase, if $-1<\omega_a<1$, the MWCNTs are concentrated at the interface, and if $\omega_a<-1$, the MWCNTs are selectively distributed in the ABS phase. The interfacial tension between the PC and ABS was calculated using the harmonic mean equation as given by equation 2,[48]

$$\gamma_{ij} = \gamma_i + \gamma_j - \frac{4\gamma_i^p \gamma_j^p}{\gamma_i^p + \gamma_j^p} - \frac{4\gamma_i^d \gamma_j^d}{\gamma_i^d + \gamma_j^d} \quad (2)$$

where γ_{ij} is the interfacial tension between components i and j, γ_i is the surface tension of component i, γ^d_i and γ^p_i are the dispersive

and polar contributions of the surface tension of component *i*, respectively. In order to calculate the interfacial tensions between MWCNTs and the blend components, the geometric mean equation of Wu, which is more suitable than the harmonic-mean equation for higher surface energies, was employed[48]:

$$\gamma_{ij} = \gamma_i + \gamma_j - 2\sqrt{\gamma_i^p \gamma_j^p} - 2\sqrt{\gamma_i^d \gamma_j^d} \quad (3)$$

In this case, *i* and *j* refer to the PC or ABS matrix and the MWCNTs, respectively. The surface tension of the blend components and MWCNTs are shown in Table 2. For this blend nanocomposite system, ω_a was found to be 0.19. Therefore thermodynamic calculations suggest that, at thermodynamic equilibrium, the MWCNTs should be preferentially localized at the interface.

Rheological measurements

Determination of the linear viscoelastic region of the samples

In order to determine the range of strain amplitude below which the linear viscoelastic behavior predominates, strain amplitude sweep experiments were performed at an angular frequency of 1 rad/s in the overall range of 0.0005–10 (0.05-1000%). The normalized storage modulus versus strain amplitude for the PC matrix, PC/ABS blend, and their nanocomposite samples containing 1 wt.% of MWCNTs is shown in Fig. 2.

As can be observed, the strain range above which the melt linear viscoelastic behavior changed to nonlinear (γ_{cr}) decreased with increasing MWCNTs content. It can also be seen that in the case of the nanocomposite samples, the transition from linear to nonlinear viscoelastic behavior occurred at a strain amplitude nearly 10 times smaller compared with the neat samples. This can be related to MWCNTs induced microstructure changes, which are highly dependent upon the imposed strain. Therefore, all the measurements were performed with an amplitude of 1%, i.e. in the linear viscoelastic region.

Dispersion of MWCNTs in blend components

The results of storage modulus and complex viscosity versus angular frequency for the PC and ABS and their nanocomposite samples containing different loadings of MWCNTs are presented in Fig. 3. It can be clearly seen that the nanocomposite samples based on the two blend components exhibit a strong solid-like behavior and a viscosity upturn at low frequency ranges whose extents increased with MWCNTs loading level. This behavior is known to be an indication of three dimensional physical networks formed between particle-particle and/or particle-matrix. The degree of dispersion and concentration of the MWCNTs determines the extent of formation of these networks. Thus, by comparing these results, one comes to the understanding that the PC has a greater capability in dispersing the MWCNTs than the ABS.[50, 51]

Normalized storage modulus and complex viscosity curves of different polymers with equal loadings of a nanofiller can provide insight about the affinity of the nanofiller towards each polymer. In the same loading levels, a stronger solid-like response in the storage modulus curve and a more remarkable viscosity upturn is an indication of stronger affinity towards that polymer. This concept was employed to cast light on the affinity of MWCNTs toward the PC and ABS. Fig. 4 presents the normalized storage modulus ($G'_{Nanocomposite}/G'_{Matrix}$) and the normalized complex viscosity ($\eta^*_{Nanocomposite}/\eta^*_{Matrix}$) versus angular frequency obtained for the PC and ABS nanocomposite samples containing 1 and 1.5 wt.% of MWCNTs. It is evident that all nanocomposite samples based on the blend components exhibited a strong MWCNTs induced solid like response at low frequencies, which was much more noticeable for the PC. From the results presented in Fig. 3 and Fig. 4, one may conclude that the MWCNTs have a much greater affinity towards the PC in comparison with the ABS.[50, 51] On the other hand, dispersive mixing of the MWCNTs in these blend components is mostly controlled by viscosity and diffusion mechanism, i.e. the rheological properties of the systems. Therefore, convective forces and kinetic parameters seem to be at work rather than thermodynamic ones.

Melt linear viscoelastic properties of blend nanocomposites

The results of storage modulus versus frequency and complex viscosity for the PC/ABS blend and its nanocomposite samples containing different loadings of MWCNTs at 260 °C are shown in Fig. 5a and b. The incorporation of MWCNTs, even at very low loading levels (the same as in Fig. 3), increased the viscosity and elasticity of the samples, which is characteristic of nanostructured materials. With increasing MWCNTs content, the non-terminal behavior in storage modulus and viscosity upturn at low frequencies became more pronounced. As mentioned above, the low frequency solid-like behavior shown by the blend nanocomposite samples is an indication of three dimensional networks formed in the matrix. Therefore, the formation of three dimensional networks in the dispersed droplets had no significant effect on changing the low frequency elastic response of the blends. It follows that melt viscoelastic experiments can provide considerable insight into understanding the localization of nanoparticles in immiscible blends. In many cases, this information can be used to assess the affinity of blend components towards MWCNTs. Interestingly, from the rheological experiments and the results shown in Fig. 5a, one can find out that a good part of the MWCNTs were localized in the PC matrix (i.e. three dimensional networks were formed in the PC matrix).

It is worth noting that the condition for using the thermodynamic model (Equation 1) is that the two blend components have comparable viscosities. Because the viscosity of the ABS is higher than the PC (Fig. 3), the thermodynamic model is not applicable to the blend nanocomposite samples and kinetic factors should be considered, which suggests that during the melt blending process, the MWCNTs first dispersed in the two blend components and then migrated toward the PC matrix, because of the higher MWCNTs diffusion coefficient in the less viscous medium of the PC. Furthermore, we can conclude that in these blend nanocomposite samples, localization of the MWCNTs was largely controlled by kinetic parameters.

The results of the damping factor (tan δ) for the PC/ABS blend and its nanocomposite samples containing different loadings of MWCNTs are shown in Fig. 5c. The blend nanocomposite samples exhibited low damping factors with a peak at a higher frequency in comparison with the blend sample, which is due to the existence of interfacial bonding between the MWCNTs and

the polymer chains. This means that the movement of the chains was restricted and that their relaxation time increased.

Morphology characterizations

SEM results

SEM micrographs of the cryofractured surfaces of the PC/ABS blend and its nanocomposite samples containing 1 and 1.5 wt.% of MWCNTs, in which the ABS phase was etched out, are presented in Fig. 6. For the blend sample (Fig. 6a), presence of the holes is a clear indication of a matrix/dispersed morphology where the ABS is dispersed in the PC matrix. As shown in Fig. 6b and c, where the arrows indicate the location of MWCNTs, the matrix/dispersed morphology of the samples remained unchanged. The blend nanocomposite samples display a good dispersion/distribution of the MWCNTs with no rich nanofiller domains and quite small aggregates, which indicates the adequacy of the mixing process.[52]

For a quantitative analysis, the number average radius $\overline{R}_n$ and volume average radius $\overline{R}_v$ of the dispersed phase were calculated by the following equations, assuming the dispersed phase in the form of spherical particles:

$$\overline{R}_n = \frac{\sum n_i R_i}{\sum n_i} \quad (4)$$

$$\overline{R}_v = \frac{\sum n_i R_i^4}{\sum n_i R_i^3} \quad (5)$$

where n_i is the number of the droplets with radius R_i. The polydispersity index (PDI) of droplet size distribution can be estimated in terms of $\overline{R}_v/\overline{R}_n$ ratio. For a monodisperse system, this ratio tends to be unity and values greater than one show broader droplet size distributions. The obtained data are summarized in Table 3. As expected, localization of MWCNTs in the PC matrix results in reduction of the ABS droplet size by suppressing the coalescence process during melt blending. Furthermore, the droplet size distribution becomes much broader in the presence of MWCNTs.

TEM results

A TEM micrograph of the PC/ABS blend containing 1 wt.% of MWCNTs is shown in Fig. 7a. The dark regions are the MWCNTs (marked by arrows), while the white regions are a result of the difference between the refractive indices of the two polymer components. As it can be observed, MWCNTs tended to localize at the interface and in the PC matrix, while the ABS droplets were nearly free of MWCNTs. This is in agreement with the rheological measurements of blend nanocomposites. Fig. 7b shows the dispersion of MWCNTs in the PC matrix. These results are consistent with the rheological measurements of nanocomposite samples, suggesting a good degree of MWCNTs dispersion in them.

Electrical properties

Electrical resistivity results

From the results discussed above, it was understood that the PC has a greater capability in dispersing the MWCNTs compared to the ABS. Therefore, the blend nanocomposite samples were expected to have an enhanced electrical conductivity. The effect of the MWCNTs on the volume resistivity of the blend nanocomposite samples is shown in Fig. 8. A sharp decline in electrical resistivity of the blend nanocomposites was evident with increasing content of MWCNTs at the low loading levels. For instance, the volume resistivity of the neat blend sample (1.3×10^{14} Ohm cm) decreased to 2.7×10^{5} Ohm cm when the MWCNTs content was increased to 0.5 wt.%. This rapid decrease (~10^{9} orders of magnitude) in electrical resistivity at 0.5 wt.% of MWCNTs loading level indicated the formation of an interconnected structure of the MWCNTs in the PC matrix, which is a well-known electrical percolation phenomenon. However, above this loading level of MWCNTs, the blend nanocomposites showed only a slow but gradual decrease in volume resistivity with increasing MWCNTs content. For example, the volume resistivity of the blend nanocomposite with 1 wt.% of MWCNTs (5.2×10^{3} Ohm cm) increased to 1.07×10^{3} Ohm cm when the MWCNTs content was increased to 1.5 wt.%. This simply means that at concentrations above 0.5 wt.% of MWCNTs, a very high percentage of the electrons were permitted to flow through the sample due to the formation of a continuous interconnecting conductive pathway.

To quantify the electrical percolation threshold, the following percolation model[53] can be used:

$$\sigma = \sigma_0 (\phi - \phi_c)^t \quad (6)$$

where σ represents volume resistivity, ϕ is the MWCNTs weight fraction, ϕ_c is the weight fraction at the percolation threshold, and t is a critical exponent. By using the above model, the value of the percolation threshold and critical exponent were estimated from the best linear fit of the log σ versus log $(\phi - \phi_c)$ plot, as shown in the inset of Fig. 8. The percolation model indicates a low percolation threshold of 0.33 wt.% of MWCNTs and the variation in σ as a function of MWCNTs content gave the best fits with a critical exponent of t=-2.87 for the blend nanocomposites.

EMI SE measurements

The results of EMI SE measurements versus frequency for the blend nanocomposite samples containing different loading levels of MWCNTs are given in Fig. 9. The EMI SE of the blend nanocomposites increased with increasing MWCNTs loading level. For the blend nanocomposite sample containing 0.5 wt.% of MWCNTs, the average EMI SE values over the 5–12 GHz range was 0.51 dB, while the samples containing 1 and 1.5 wt.% of MWCNTs showed average EMI SE values of 1.33 and 1.98 dB, respectively. These results showed that the blend nanocomposite samples with lower electrical resistivity achieved higher EMI SE. A maximum EMI SE of almost 2.2 dB was obtained in case of the sample containing 1.5 wt.% of MWCNTs at average frequencies over 11-12 GHz.

EMI SE is strongly dependent on the dispersion degree of MWCNTs in the polymer matrix. The incorporation of the MWCNTs, which have a high aspect ratio and a low percolation threshold and thus, require lower loading levels for EMI SE, can enhance absorption and reflection as the primary and secondary shielding mechanisms. The contribution of absorption to the total EMI SE was more than that of reflection, which was attributed to the presence of internal cavity of the MWCNTs. Therefore,

MWCNTs based nanocomposites show excellent promise for developing strong EMI shielding materials.[54, 55] Similar results have also been reported by Al-saleh et al.[56] demonstrating that the EMI SE of MWCNTs based nanocomposites is significantly higher than that of carbon nanofibers and carbon black based nanocomposites.

Thermal analyses

Dynamic mechanical behavior of samples

Dynamic mechanical analysis is a powerful characterization tool to understand the dynamic response of samples.[57] The results of damping factor (tan δ) versus temperature for the PC, ABS and PC/ABS blend at 1 Hz are shown in Fig. 10. As it can be observed, the ABS and PC each showed a single peak, corresponding to their T_gs, at ~105 °C and ~140 °C, respectively. Furthermore, T_gs of the PC and ABS shift towards one another in the blend sample suggesting a partial miscibility between the two blend components.

The results of storage modulus (E') and damping factor (tan δ) versus temperature for the PC/ABS blend and its nanocomposite samples containing different loading levels of MWCNTs are given in Fig. 11. As it can be seen from Fig. 11a, the incorporation of MWCNTs into the blend resulted in a slight increase in the storage modulus. Based on this observation, we suggest that incorporation of MWCNTs results in formation of cross-linking physical bonds between the PC chains and MWCNTs and thus the movement of chains is restricted and the storage modulus of the blend nanocomposites increased. From Fig. 11b, it can be seen that with the incorporation of MWCNTs into the blend, additional energy dissipation occurred and the tan δ peak area (the height) decreased. Furthermore, it was found that influence of MWCNTs incorporation on the PC matrix was stronger compared to ABS in terms of reducing chains' mobility, and consequently, there was a small increase in the T_g of the PC matrix. These results indicated the presence of more MWCNTs in the PC matrix, which is in good agreement with the rheology and TEM results.

Thermal stability study

Thermal stability dependence of blend nanocomposite samples on MWCNTs content was investigated by thermogravimetric and differential thermogravimetric analysis (TG-DTA) and the obtained results presented in Fig. 12. The relative thermal stability of the samples was compared by means of the temperature of 5% ($T_{d,5\%}$, temperature corresponds to 5% loss) and 70% weight loss ($T_{d,70\%}$, temperature corresponds to 70% loss), the temperature of maximum rate of mass loss (T_{max}), and the char yields at 550 °C. The thermogravimetric data are summarized in Table 4. The neat blend had a two-step decomposition process, representing the degradation of the ABS and PC components, respectively. As for blend nanocomposites, the first decomposition step nearly disappeared, being a shoulder, and the $T_{d,5\%}$ was slightly smaller than that of the neat blend. The decrease of $T_{d,5\%}$ is due to the higher thermal conductivity of MWCNTs and the consequently better heat transfer to the dispersed phase, i.e. ABS. The $T_{d,70\%}$ and thermal stability were enhanced by the addition of the MWCNTs. T_{max} of the blend nanocomposites were also higher than that of the neat blend, indicating that incorporation of MWCNTs effectively improved the thermal stability of the nanocomposites. This improved thermal stability is due to the known protective effect (mass transfer barrier) of the MWCNTs against thermal decomposition of the nanocomposites. It was also observed that much more residual char was obtained for the blend nanocomposites compared with neat blend sample.

Table 1. The commercial details and properties of the polymers used

Polymer	Supplier	Grade	Melt Flow Index	Density
PC	Bayer Co., Germany	Makrolon 2858	10 (300 °C, 1.2 kg)	1.2 g/ml
ABS	Tabriz Petrochemical Co., Iran	SD 0150	5 (200 °C, 5 kg)	1.04 g/ml

Table 2. The surface tension of the sample components (the fraction of total, dispersive and polar contributions) calculated at 260 °C

	γ (mN/m)	γ^d (mN/m)	γ^p (mN/m)
PC	37.5	31.7	5.8
ABS	27.91	26.49	1.33
MWCNTs	45.3	18.4	26.9

Table 3. The values of the droplet size and polydispersity for PC/ABS blend and its nanocomposite sample containing 1 and 1.5 wt.% of MWCNTs on the basis of a quantitative analysis on SEM micrographs

Samples	$\overline{R}_n$ (μm)	$\overline{R}_v$ (μm)	PDI
PC/ABS	2.77	3.07	1.11
PC/ABS-1%MWCNTs	1.16	1.71	1.47
PC/ABS-1.5%MWCNTs	0.91	1.81	1.99

Table 4. TG-DTA data for the blend samples containing different loading levels of MWCNTs

Samples	$T_{d,5\%}$ (°C)	$T_{d,70\%}$ (°C)	T_{max} (°C)	Char residue (%) at 550 °C
PC/ABS	396.6	464.2	417.9, 444.9	17.6
PC/ABS-0.5%MWCNTs	392.5	467.6	448.1	19.9
PC/ABS-1%MWCNTs	391.9	469.4	451.9	21.4
PC/ABS-1.5%MWCNTs	392	473.9	452	25.2

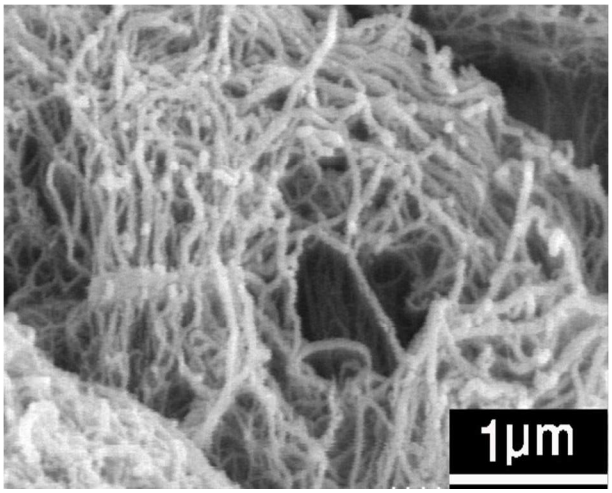

Fig. 1 SEM micrograph of the MWCNTs used

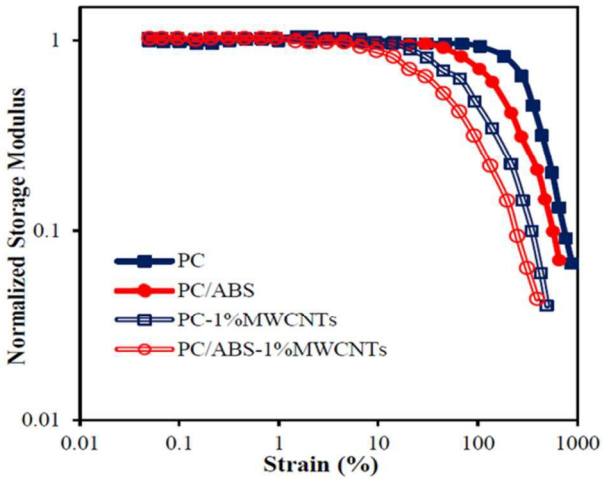

Fig. 2 Normalized storage modulus versus strain amplitude for the neat PC and PC/ABS samples and their corresponding nanocomposites

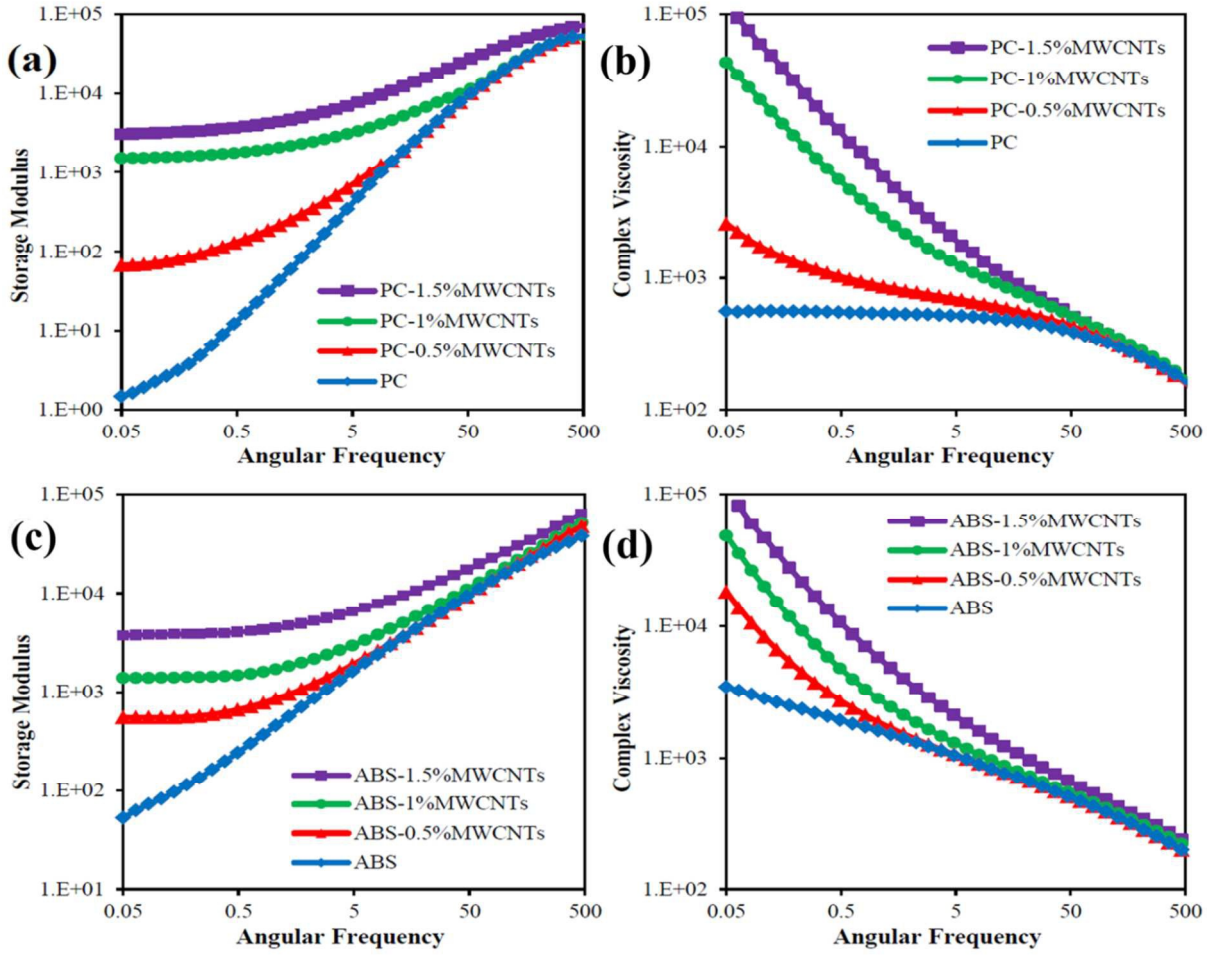

Fig. 3 Effect of MWCNTs content on the storage modulus and complex viscosity of PC (a, b) and ABS (c, d) obtained at 260 °C

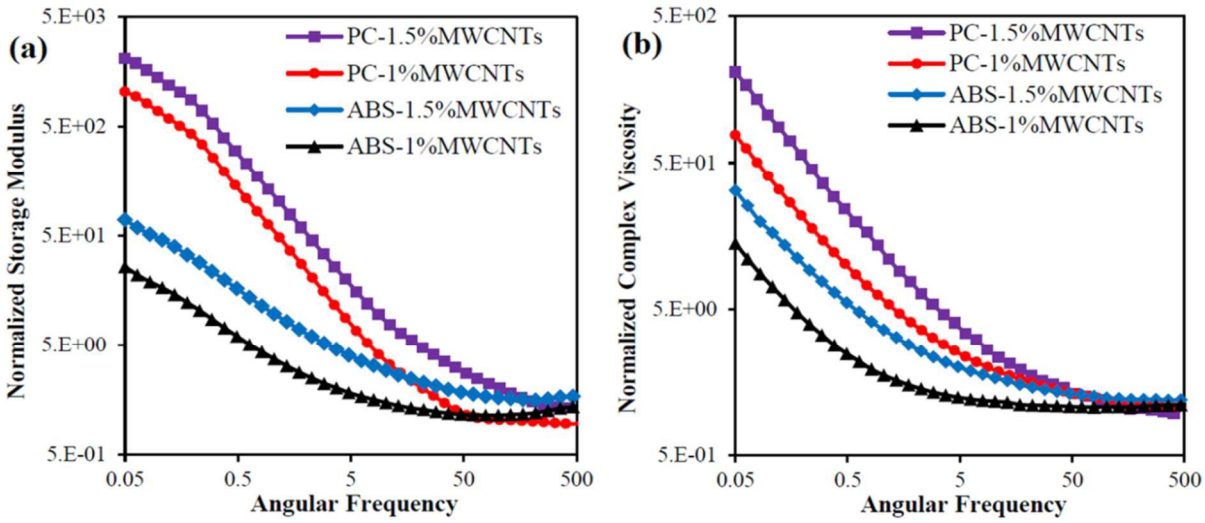

Fig. 4 (a) Normalized storage modulus and (b) normalized complex viscosity versus angular frequency for the PC and ABS nanocomposite samples containing 1 and 1.5 wt.% of MWCNTs

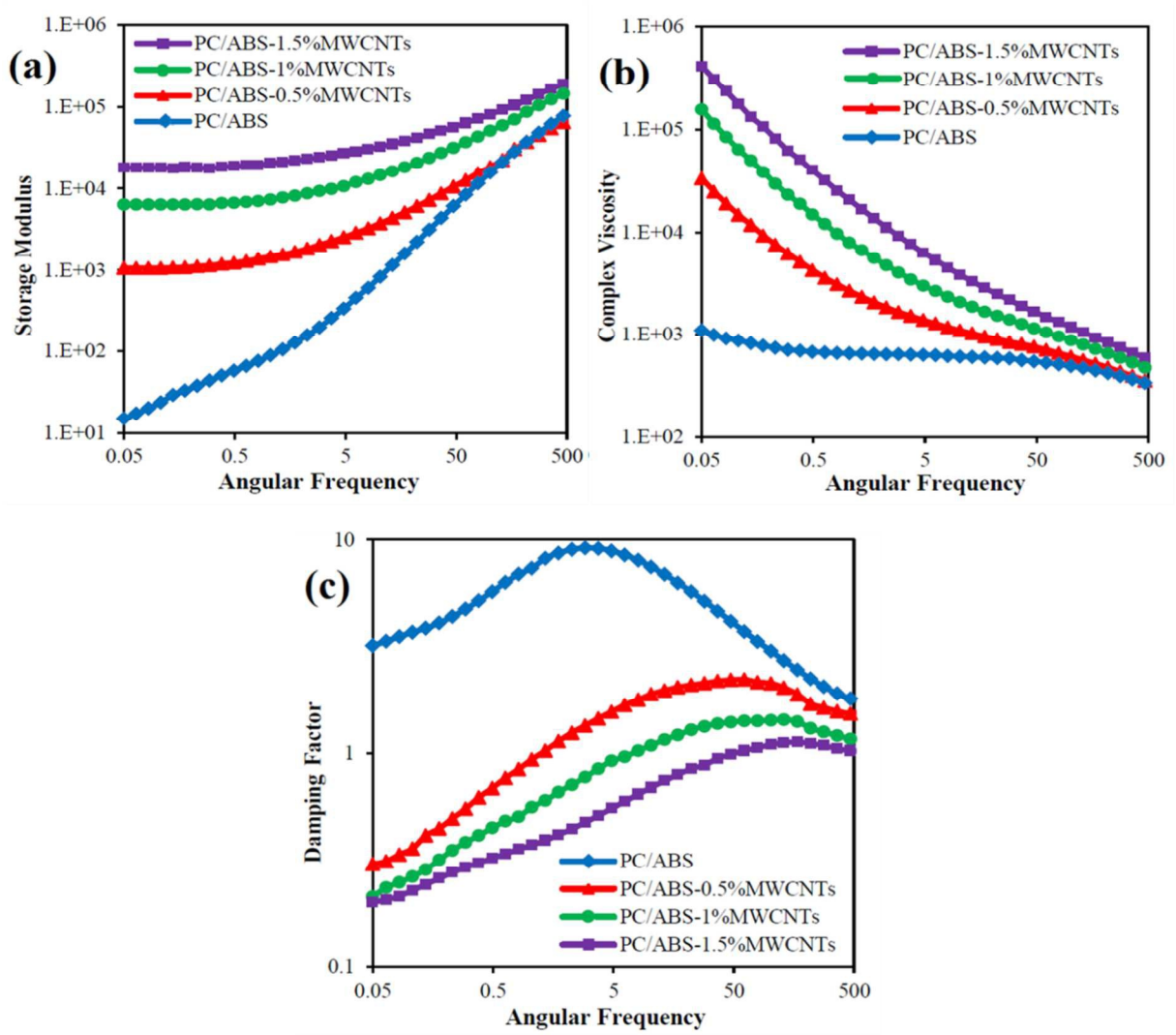

Fig. 5 Effect of MWCNTs content on (a) storage modulus, (b) complex viscosity, and (c) damping factor of the PC/ABS blend at 260 °C

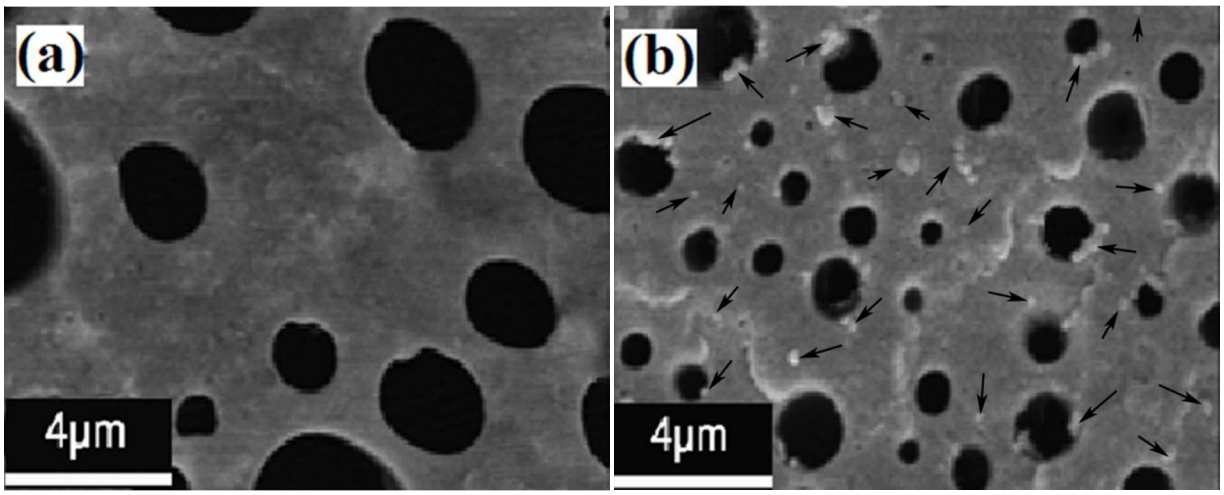

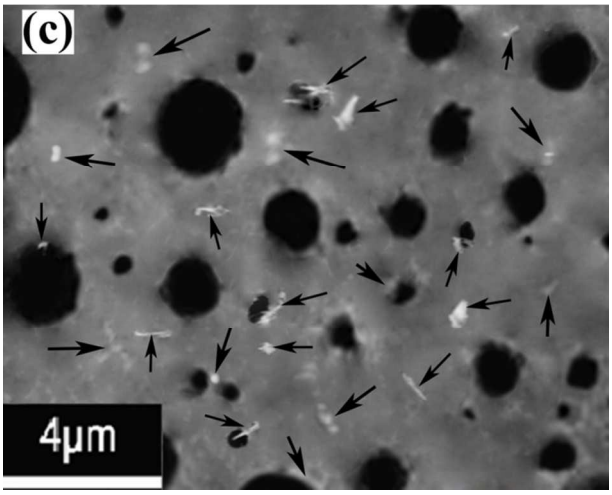

Fig. 6 SEM micrographs of the cryofractured surface of the PC/ABS blend containing (a) 0 wt.% of MWCNTs, (b) 1 wt.% of MWCNTs, and (c) 1.5 wt.% of MWCNTs. The arrows indicate the location of the MWCNTs.

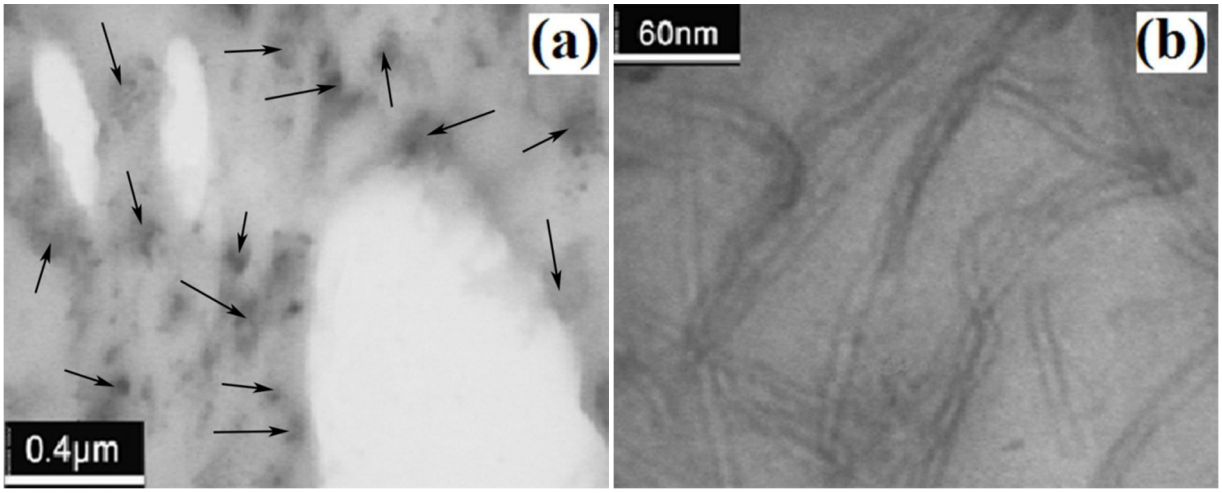

Fig. 7 TEM micrographs showing (a) the PC/ABS blend in the presence of 1 wt.% of MWCNTs and (b) dispersion state of the MWCNTs in the PC matrix. The arrows mark the presence of MWCNTs in the dark regions.

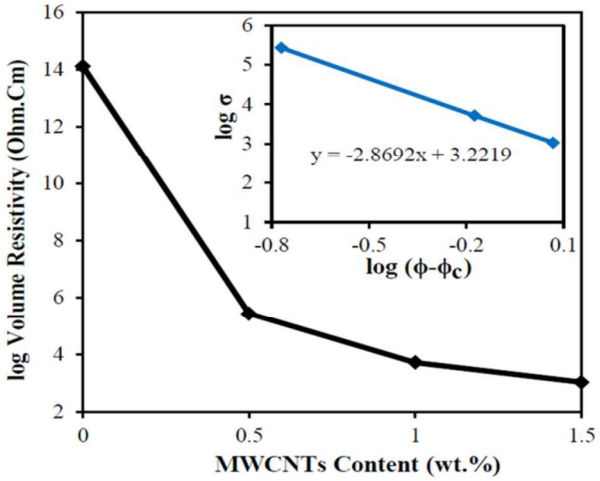

Fig. 8 The effect of MWCNTs content on volume resistivity of the PC/ABS blend nanocomposite samples. The best linear fit of the log σ versus log $(\phi - \phi_c)$ plot is shown in the inset.

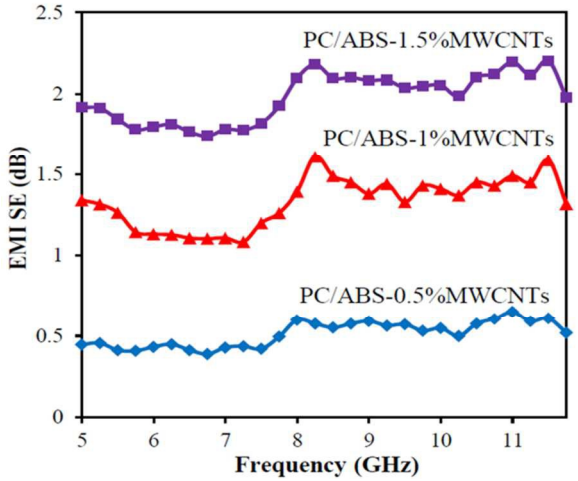

Fig. 9 The effect of MWCNTs content on EMI SE of the PC/ABS blend nanocomposite samples

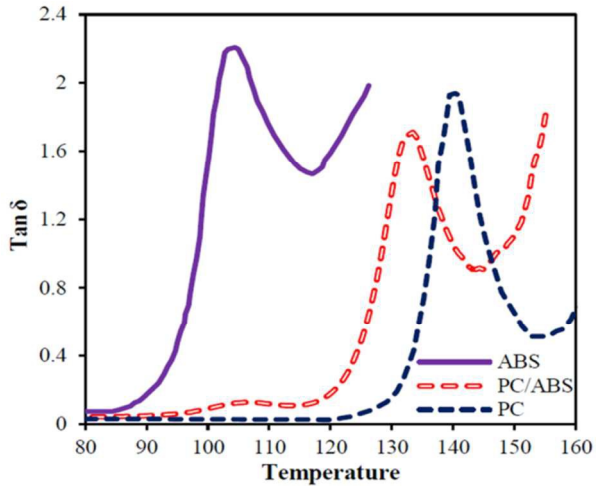

Fig. 10 Damping factor versus temperature for PC, ABS, and the PC/ABS blend

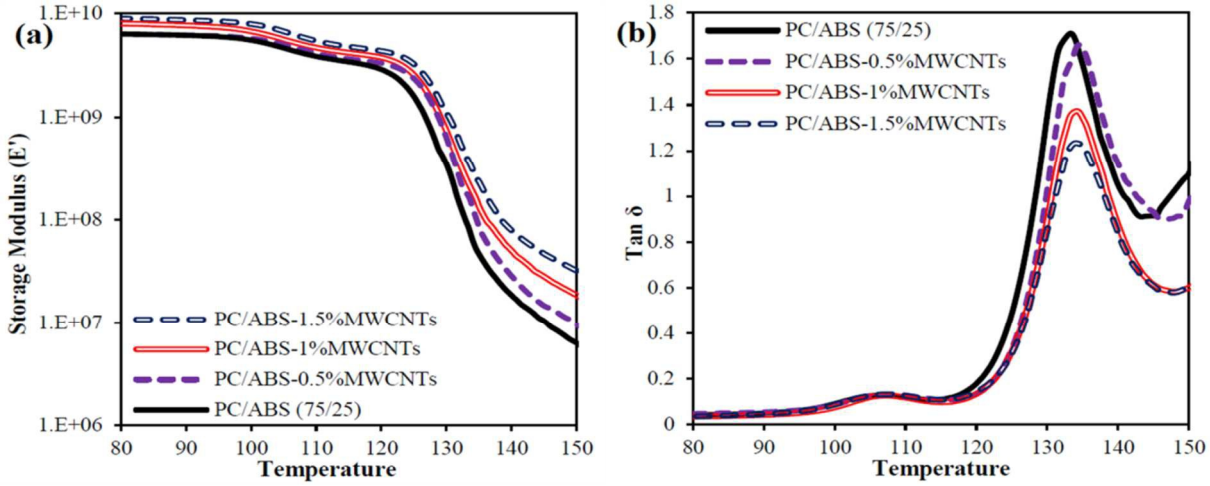

Fig. 11 DMA plots of (a) storage modulus and (b) damping factor for the PC/ABS blend and its nanocomposites containing different loadings of MWCNTs

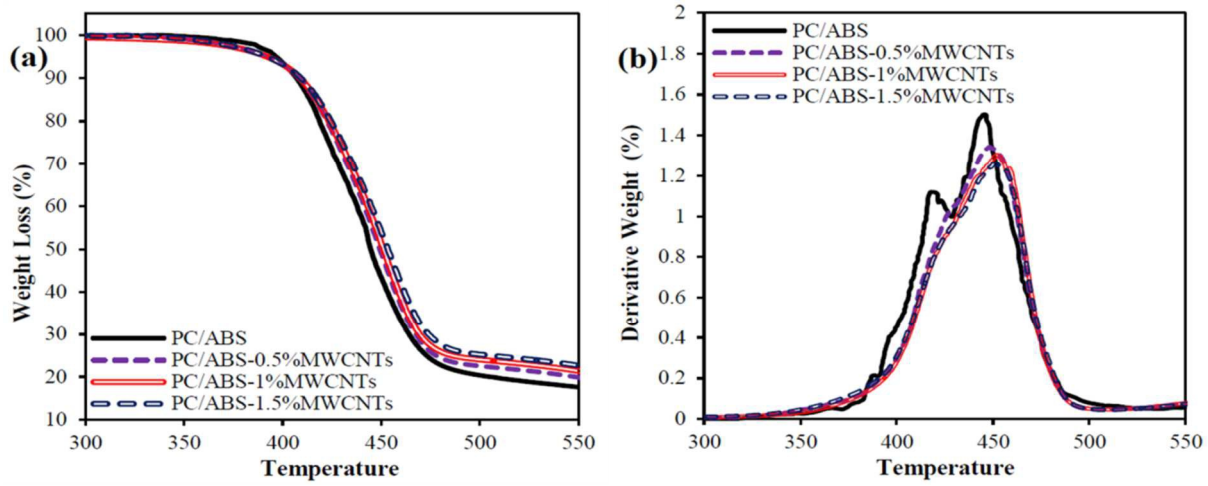

Fig. 12 (a) TGA and (b) DTA curves of the PC/ABS blend containing different loading levels of MWCNTs

Conclusions

In this study, we investigated the rheological, electrical, and thermal properties of the PC/ABS (75/25)/MWCNTs blend nanocomposites. It was demonstrated that the localization of the MWCNTs was controlled by a combination of thermodynamic and kinetic parameters. From the rheological measurements and TEM results, the MWCNTs appeared to be more localized in the PC matrix because of the kinetic driving force, although thermodynamic studies suggested that MWCNTs concentrated at the interface. SEM showed that the blend morphology (dispersed ABS domains in the PC matrix) did not change with incorporation of MWCNTs and it was found that droplet size of the ABS was slightly reduced. Furthermore, TEM micrographs revealed good dispersion and distribution of the MWCNTs in the blend matrix. Percolation threshold of the electrical conductivity was calculated to occur at 0.33 wt.% of MWCNTs. The electrical conductivity and EMI SE of the blend nanocomposite samples were enhanced with increasing MWCNTs loading levels and the EMI SE values were greater at higher frequencies. DMA results of the blend nanocomposite samples showed a noticeable decrease in the damping of the PC phase. The restricted motion of the PC chains was due to the presence of a large part of the MWCNTs in this phase, which is in good agreement with the results obtained by rheology and TEM. The TGA results indicated that the incorporation of MWCNTs into the blend improved the thermal stability and the char yields of the blend nanocomposites compared with the neat blend.

Notes and references

[a] *Department of Polymer Engineering, Islamic Azad University, Mahshahr Branch, Khuzestan-Iran.* Tel: +98 9132755096; *Email: rostamy_amir@yahoo.com; Email: Mo_masoomi@yahoo.com; Email: mohammadfayazi065@yahoo.com.*

[b] *Department of Polymer Engineering, Amirkabir University of Technology-Mahshahr Campus, Khuzestan-Iran. Email: mvahdaty@yahoo.com.*

1. D. Paul and S. Newman, *Polymer blends, vols. 1 and 2*, New York, 1978.
2. S. Akiyama, T. Inoue and T. Nishi, *Polymer Blends; Miscibility and Interface*, Tokyo, 1981.
3. L. Utracki, *Polymer alloys and blends* Munich, 1989.
4. R. Greco, M. F. Astarita, L. Dong and A. Sorrentino, *Advances in Polymer Technology*, 1994, **13**, 259-274.
5. R. Greco and A. Sorrentino, *Advances in Polymer Technology*, 1994, **13**, 249-258.
6. Z. Tan, X. Xu, S. Sun, C. Zhou, Y. Ao, H. Zhang and Y. Han, *Polymer Engineering & Science*, 2006, **46**, 1476-1484.
7. H. T. Pham, C. L. Weckle and J. Ceraso, *Advanced Materials*, 2000, **12**, 1881-1885.
8. D. R. Paul and L. M. Robeson, *Polymer*, 2008, **49**, 3187-3204.
9. J. Jordan, K. I. Jacob, R. Tannenbaum, M. A. Sharaf and I. Jasiuk, *Materials Science and Engineering: A*, 2005, **393**, 1-11.
10. M. Rahmat and P. Hubert, *Composites Science and Technology*, 2011, **72**, 72-84.
11. Z. Spitalsky, D. Tasis, K. Papagelis and C. Galiotis, *Progress in Polymer Science*, 2010, **35**, 357-401.
12. F. Tao, B. Nysten, A.-C. Baudouin, J.-M. Thomassin, D. Vuluga, C. Detrembleur and C. Bailly, *Polymer*, 2011, **52**, 4798-4805.
13. J. Bouchard, A. Cayla, E. Devaux and C. Campagne, *Composites Science and Technology*, 2013, **86**, 177-184.
14. Q. Cheng, J. Bao, J. Park, Z. Liang, C. Zhang and B. Wang, *Advanced Functional Materials*, 2009, **19**, 3219-3225.
15. Q. Cheng, M. Li, L. Jiang and Z. Tang, *Advanced Materials*, 2012, **24**, 1838-1843.
16. S. Bose, A. R. Bhattacharyya, P. V. Kodgire and A. Misra, *Polymer*, 2007, **48**, 356-362.
17. S. Bose, A. R. Bhattacharyya, A. P. Bondre, A. R. Kulkarni and P. Pötschke, *Journal of Polymer Science Part B: Polymer Physics*, 2008, **46**, 1619-1631.
18. S. Bose, A. R. Bhattacharyya, A. R. Kulkarni and P. Pötschke, *Composites Science and Technology*, 2009, **69**, 365-372.
19. G. Chen, J. Lu and D. Wu, *Materials chemistry and physics*, 2007, **104**, 240-243.
20. J. Chen, Y.-y. Shi, J.-h. Yang, N. Zhang, T. Huang, C. Chen, Y. Wang and Z.-w. Zhou, *Journal of Materials Chemistry*, 2012, **22**, 22398-22404.
21. M. Ji, H. Deng, D. Yan, X. Li, L. Duan and Q. Fu, *Composites Science and Technology*, 2014, **92**, 16-26.

22. Z. Jin, K. Pramoda, S. H. Goh and G. Xu, *Materials Research Bulletin*, 2002, **37**, 271-278.
23. R. A. Khare, A. R. Bhattacharyya, A. R. Kulkarni, M. Saroop and A. Biswas, *Journal of Polymer Science Part B: Polymer Physics*, 2008, **46**, 2286-2295.
24. R. A. Khare, A. R. Bhattacharyya and A. R. Kulkarni, *Journal of Applied Polymer Science*, 2011, **120**, 2663-2672.
25. X.-Q. Liu, W. Yang, B.-H. Xie and M.-B. Yang, *Materials & Design*, 2012, **34**, 355-362.
26. M. Mukherjee, T. Das, R. Rajasekar, S. Bose, S. Kumar and C. Das, *Composites Part A: Applied Science and Manufacturing*, 2009, **40**, 1291-1298.
27. P.-C. Ma, N. A. Siddiqui, G. Marom and J.-K. Kim, *Composites Part A: Applied Science and Manufacturing*, 2010, **41**, 1345-1367.
28. C. Su, L. Xu, C. Zhang and J. Zhu, *Composites Science and Technology*, 2011, **71**, 1016-1021.
29. A.-C. Baudouin, J. Devaux and C. Bailly, *Polymer*, 2010, **51**, 1341-1354.
30. R. Sengupta, M. Bhattacharya, S. Bandyopadhyay and A. K. Bhowmick, *Progress in Polymer Science*, 2011, **36**, 638-670.
31. A. Göldel, G. Kasaliwal and P. Pötschke, *Macromolecular rapid communications*, 2009, **30**, 423-429.
32. A. Göldel, A. Marmur, G. R. Kasaliwal, P. Pötschke and G. Heinrich, *Macromolecules*, 2011, **44**, 6094-6102.
33. X. Zhao, J. Zhao, J.-P. Cao, D. Wang, G.-H. Hu, F. Chen and Z.-M. Dang, *Materials & Design*, 2014, **56**, 807-815.
34. L. Zonder, A. Ophir, S. Kenig and S. McCarthy, *Polymer*, 2011, **52**, 5085-5091.
35. Y. Mamunya, *Macromolecular Symposia*, 2001, **170**, 257-264.
36. F. Fenouillot, P. Cassagnau and J. C. Majesté, *Polymer*, 2009, **50**, 1333-1350.
37. A. Taguet, P. Cassagnau and J.-M. Lopez-Cuesta, *Progress in Polymer Science*, 2014, **39**, 1526–1563.
38. O. Koysuren, S. Yesil and G. Bayram, *Journal of Applied Polymer Science*, 2010, **118**, 3041-3048.
39. J. Huang, C. Mao, Y. Zhu, W. Jiang and X. Yang, *Carbon*, 2014, **73**, 267-274.
40. Y. Sun, Z. X. Guo and J. Yu, *Macromolecular Materials and Engineering*, 2010, **295**, 263-268.
41. Z.-Y. Xiong, L. Wang, Y. Sun, Z.-X. Guo and J. Yu, *Polymer*, 2013, **54**, 447-455.
42. S. Maiti, N. K. Shrivastava and B. Khatua, *Polymer Composites*, 2013, **34**, 570-579.
43. S. Taheri, E. Nakhlband and H. Nazockdast, *Polymer-Plastics Technology and Engineering*, 2013, **52**, 300-309.
44. S. Monemian, S. H. Jafari, H. A. Khonakdar, V. Goodarzi, U. Reuter and P. Pötschke, *Journal of Applied Polymer Science*, 2013, **130**, 739-748.
45. I.-S. Han, Y. K. Lee, H. S. Lee, H. G. Yoon and W. N. Kim, *Journal of Materials Science*, 2014, **49**, 4522-4529.
46. E. Nazockdast, H. Nazockdast and F. Goharpey, *Polym. Eng. Sci.*, 2008, **48**, 1240-1249.
47. M. Wang, W. Wang, T. Liu and W.-D. Zhang, *Composites Science and Technology*, 2008, **68**, 2498-2502.
48. S. Wu, *Polymer interface and adhesion*, New York, 1982.
49. M. Sumita, K. Sakata, S. Asai, K. Miyasaka and H. Nakagawa, *Polymer bulletin*, 1991, **25**, 265-271.
50. F. Goharpey, H. Nazockdast and A. A. Katbab, *Polym. Eng. Sci.*, 2005, **45**, 84-94.
51. A. Saadat, H. Nazockdast, F. Sepehr and M. Mehranpour, *Polym. Eng. Sci.*, 2010, **50**, 2340-2349.
52. Q. Cheng, J. Wang, K. Jiang, Q. Li and S. Fan, *Journal of Materials Research*, 2008, **23**, 2975-2983.
53. R. Vargas-Bernal, G. Herrera-Pérez, M. E. Calixto-Olalde and M. Tecpoyotl-Torres, *Journal of Electrical and Computer Engineering*, 2013, **2013**.
54. M. H. Al-Saleh and U. Sundararaj, *Carbon*, 2009, **47**, 1738-1746.
55. M. Mahmoodi, M. Arjmand, U. Sundararaj and S. Park, *Carbon*, 2012, **50**, 1455-1464.
56. M. H. Al-Saleh, W. H. Saadeh and U. Sundararaj, *Carbon*, 2013, **60**, 146-156.
57. K. P. Menard, *Dynamic mechanical analysis: a practical introduction*, Florida, 2008.